Indian Journal of Pure & Applied Physics
Vol. 64, May 2026, pp. 502-518
DOI: 10.56042/ijpap.v65i5.27294

Optimization of Optimal Gain Ultra Wide Band Microstrip patch antenna for C-Band, X-Band and Ku-Band Application

Rajesh Kumar Nema[a*], Anubhuti Khare[b], Puran Gour[c], Preeti Verma[a], Kavita Barahar[a], Amit Kumar Nema[d] & Veena Upadhyay[e]

[a]Department of Electronics and Communication Engineering, IES College of Technology, Bhopal 462 044, India

[b]Department of Electronics and Communication Engineering, University Institute of Technology RGPV, Bhopal 462 033, India

[c]Department of Electronics and Communication Engineering, NRI College of Technology, Bhopal 462 022, India

[d]Department of Education, Rabindranath Tagore University, Bhopal 464 993, India

[e]Department of Electronics and Communication Engineering, IES University, Bhopal 462 044 , India

Received: 22nd January 2026; accepted: 30th March 2026

In this paper, the optimization of an ultra-wideband optimal gain parasitic circularly polarized patch antenna for C-Band, X-Band, and Ku-Band applications has been presented. The proposed geometry of the antenna is designed using a negative mutual coupling approach and parasitic array techniques. The geometrical structure has been configured by a ground plane, driven element, and top layer U- slot director. The greenhouse analysis is being used for the calculation of total inductance and mutual inductance of the geometries. The gap coupling and negative mutual approaches have been used for enhancing the gain and impedance bandwidth of the designed antenna. The novel U-shaped directors have been used to improve the radiation characteristics of the antenna. The optimization of the antenna is discussed in five sections. The mathematical modeling of inductance and mutual inductance has been done for an appropriate solution. After all optimizations, the optimum antenna design has been found, providing an operating impedance bandwidth and optimal gain from 5. 8 GHz to 18.15 GHz. The proposed parasitic array antenna has been designed with appropriate dimensions and can be used for X-Band, Ku-Band, and C-Band wireless communication. The simulated antenna has been fabricated and validated experimentally.

Keywords: Parasitic array, Negative mutual coupling, Mutual coupling reduction technique, Green house analyses

1 Introduction

Microstrip antennas motivate researchers to investigate various possible configurations of the antenna to satisfy recent requirements while facing issues of mutual inductance, low gain, and narrow bandwidth. Simultaneously, there is a need for improvement in the axial ratio bandwidth and impedance bandwidth. To reduce these issues, this paper presents a mutual inductance reduction technique using greenhouse analysis. In microstrip antenna design, the inductance of geometry plays a significant role in providing mutual coupling and impedance bandwidth. The total inductance of the antenna consists of three parts: self-inductance, positive mutual inductance, and negative mutual inductance. A large number of studies have been conducted in the past decade; several mutual coupling methods are used for optimizing the total inductance of the geometry. The performance of antennas is degraded due to self -inductance and mutual inductance.

2 Literature Review

In the past decade, various techniques have been employed to reduce the mutual inductance of antennas. The infinitesimal dipole model (IDM) was discussed to analyze mutual coupling across antenna structures and provides significant results, also demonstrating radiation characteristics[1]. The high-gain microstrip antenna based on a metasurface antenna that can be used in wideband applications[2]. The multiband L-slot microstrip antenna that could support multiple wireless communication bands[3]. The other method that has been examined extensively is the application of metasurfaces and metamaterial arrays to boost the gain and bandwidth of the antenna. A parasitic patch antenna with a defected ground structure (DGS) was suggested to enhance the bandwidth of impedance and radiation efficiency[4]. Similarly, the hybrid slot antenna was proposed has

*Corresponding author: E-mail: rajeshnema20018@gmail.com

the potential to support ultra-wideband communication systems with enhanced bandwidth qualities[5]. The patch antenna with slot loading was shown to produce a dual patch wideband microstrip antenna that had a high operating bandwidth[6]. The gain of a microstrip antenna was improved through dielectric substrate layers[7]. Additionally, the small wideband microstrip antennas that can be used in modern wireless communication practices were discussed[8]. The antenna impedance matching was further enhanced for the broadband U-Shaped Director configuration[9]. The inductive microstrip lines and capacitive slot hybrid techniques were used to develop antenna structures that significantly reduced the mutual coupling effect by generating different values of inductance and capacitance[10]. The 5G and beyond antenna was developed using a 45° angled inclined dipole structure with a balun to reduce mutual coupling across the antenna structure[11]. The challenges, issues, and proposed solutions related to mutual coupling across various wireless communication systems and also analyzed the radiation characteristics of a 2×1 linear microstrip antenna array[12]. The E-type patch antenna; the complementary U-shaped polarization converter was used to reduce mutual coupling across the antenna geometry, achieving a gain up to 8 dB with a structure designed with the distance between elements at $0.1\lambda_o$[13]. The dual-band U-Shaped Director microstrip antenna in 5G with an antenna modified ability that altered the bandwidth and radiation properties[14]. The other method that has been examined extensively is the application of metasurfaces and metamaterial arrays to boost the gain and bandwidth of the antenna. The different design of a metasurface-based MIMO antenna was developed that had better gain and bandwidth performance[15]. Some other researchers have studied other antenna structures and gain enhancement methods. The wideband quasi-Yagi antenna for wireless communication systems with enhanced radiation functions. Hybrid antenna systems have more recently been explored to allow for ultra-wideband performance[16]. The initial works on optimization of microstrip patch antennas operating in C, X, and Ku bands were carried out for improving bandwidth and gain[17, 18]. Simultaneously, the pioneering work of on lumped elements offers important background information on RF and microwave circuit design. Their works explain how lumped components behave, couple, and are implemented in integrated circuits, and are the theoretical foundation to current antenna and circuit integration[19]. Early works of Greenhouse experimented with inductive element design and properties and their use in microwave integrated circuits[20], recent research trends are more towards reconfigurable and multifunctional antenna systems. Innovative designs were discussed which include circularly polarized reconfigurable patch antennas, metamaterial-based IoT absorbers[21-22], Overall, the literature shows that there is a clear transition between simple optimization and theoretical modeling to complex, reconfigurable and application-specific antenna designs. The incorporation of metamaterials, reconfigurability, and multi-bands highlights the changing needs of the latest wireless communication systems, where efficiency, flexibility, and miniaturization are paramount.

3 Methodology

3.1 Proposed Antenna Design

The theory of parasitic antenna array is used for the design of the geometry. The proposed antenna has been constructed with three elements: a ground plane, driven elements, and directors shown in Fig. 1.

The proposed geometry consists of:

i The glass epoxy PCB dielectric constant and air gap (FR-4 - air - FR-4).

ii The dimensions of the ground plane are chosen as 1137 x 1172 mil² (0.5λ x 0.5154λ mil² reflector) for the optimum reduction in the mutual coupling across the geometry.

iii The spacing distance is 0.29λ between the ground plane and the driven element.

iv The spacing distance is 0.308λ between the driven element and the director.

v The middle layer driven element has been designed with dimensions L x W = 411 x 446 mil² (0.1808λ x 0.1962λ mil² driven elements).

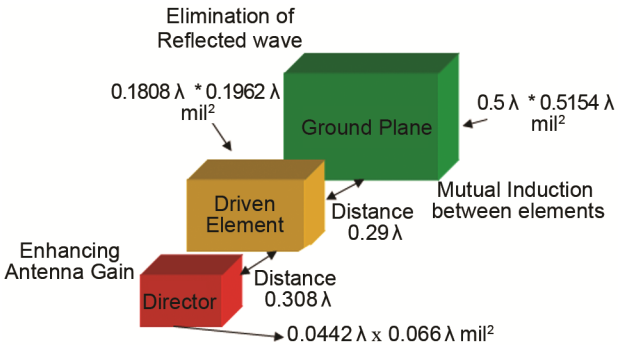

Fig. 1 — Proposed Model

vi The total height of the designed antenna is 121 mil.

vii The top parasitic director is designed with dimensions L_1 x W_1 = 100 x 150 mil² (0.044λ x 0.066λ mil²).

viii The top layer director has been optimized in five antenna configurations.

The proposed reflector ground plane is designed with dimensions of 0.5λ*0.5154λ mil^2. This specific dimension causes a 180-degree phase shift, which helps convert most of the reflected wave into a forward wave and achieves good impedance matching. The driven element has dimensions of 0.1808λ * 0.1962λ mil^2, providing a 70-degree phase shift. This allows most of the incident signal to move forward, improving the impedance matching bandwidth and the gain of the antenna. It is known that to achieve maximum gain, the phase shift inside the antenna structure should be 90 degrees. In this design, the gain and bandwidth of the antenna are enhanced at the same time. The -10dB impedance bandwidth and the 3dB axial ratio bandwidth have both been improved simultaneously. The spacing between the elements is chosen based on the design principles of a Yagi-Uda antenna. The spacing between the elements is D_1 = 0.308λmil and D_2 = 0.29λmil, which results in approximately a 10-degree phase shift within the antenna structure. This reduces signal reflection and path losses between the elements, and increases the antenna's directivity. The U-shaped director is designed to have dimensions of 0.044λ * 0.066λ mil^2 and provides a 13-degree phase shift.

The Self and mutual inductance optimization techniques are implemented in the U-shaped director. An air gap of 3 mils has been inserted between two FR-4 layers to enhance impedance matching over a wide frequency range. The design of the proposed antenna has been optimized in five sections, with attention to the ground plane using greenhouse theory. The improved bandwidth and gain of the antenna are achieved through the use of a parasitic U-Shaped director with negative mutual coupling. The negative mutual coupling is configured using greenhouse analysis. The currents generated on the adjacent U-shape parasitic director are caused by the electromagnetic fields from the driven radiating patch. Due to the proper arrangement of the slot geometry and positioning, the induced current on the parasitic element is in the opposite direction to the current on the driven element, resulting in negative mutual coupling between the elements. This negative coupling helps regulate and enhance the effective input impedance of the antenna, which improves the impedance matching over a broader frequency range. As a result, multiple resonant modes are generated, contributing to the formation of a wide impedance bandwidth. The U-shaped director also serves as a radiating component, re-emitting the electromagnetic energy that has been coupled. The driven patch radiates in the forward direction, which strengthens the parasitic director's radiation field and increases the overall gain and radiation efficiency of the antenna. Furthermore, the new surface current distribution adds an extra length to the effective current path on the antenna, which contributes to its ultra-wideband performance across the C-, X-, and Ku-bands.

3.2 Mutual Coupling Approach for Designing of Proposed Antenna (Green House Analysis)

The Greenhouse analytical model[20] was used for the mathematical modeling of the proposed antenna. The self-inductance, as well as positive and negative mutual inductances, was calculated both with and without the presence of the ground plane. Equations (1) - (6).

$$L_{Total} = \Sigma L + \Sigma M_{+} - \Sigma M_{-} - L_{mg} \quad \ldots (1)$$

where

L_{Total} = Overall calculated inductance of the microstrip antenna

ΣM_{+} = Total calculated Positive value of mutual inductance

ΣM_{-} = Total calculated Negative value of the mutual inductance

ΣL = Total computation value ofSelf Inductance

3.3 Analytical Models for Self-inductance, Surface Resistance and Capacitance using Greenhouse Analysis

The self-inductance, surface resistance, and capacitance are calculated using Greenhouse analysis[19-20]

$$L(nH) = 2\times10^{-4} l\left[In\left(\frac{l}{W+t}\right) + 1.193 + \frac{W+t}{3l}\right] K_g \text{-} \quad \ldots (2)$$

$$K_g = 0.57 - 0.145\frac{W}{h} \quad \ldots (3)$$

where $\frac{W}{h} > 0.05$

$$C = 16.67\times10^{-4} l \frac{\sqrt{\varepsilon_{eff}}}{Z_0} \quad \ldots (4)$$

$$R_s(\Omega) = \frac{KR_{sh}l}{2(W+t)} \quad \ldots (5)$$

$$K = 1 + 0.333\left(1 + \frac{d}{W}\right) \quad \ldots (6)$$

The coefficient Kg is an aspect that contributes to the impact of ground plane. The value of Kg is 1 when there is no ground plane and it reduces as the ground plane approaches the radiating patch. K is a correction factor, which determines the coroner current of the radiating patch. Where W, t, h, l and Rsh are the line width, line thickness, substrate thickness, length of the section and the sheet resistance per square of the conductor respectively. The proposed antenna minimizes the mutual inductance of the geometry. The U-shape director creates negative mutual coupling through the vertical arms of the U-Shaped Director has shown in Fig. 2.

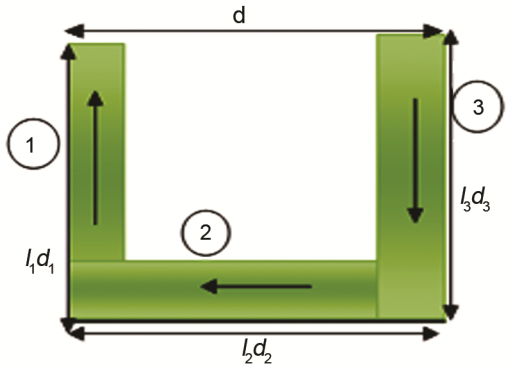

Fig. 2 — Structure of Proposed U-Shape radiating Patch (Director)

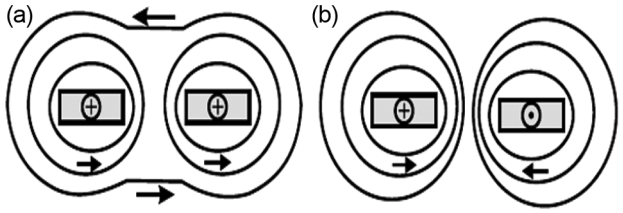

Fig. 3 — (a) Positive Mutual Coupling; and (b) Negative Mutual Coupling

The current flowing in the same way in two sections has positive mutual inductance and the current flowing in opposite directions has negative mutual inductance as represented in Fig. 3. Extensive downward paths that the added rims offer explain the extension of the effective patch current paths. This implies that the radiation properties of this small design can be just as good as that of a standard patch antenna with a planar radiating patch. The frequencies at which adjacent resonant modes can be excited are similar and hence the radiation characteristics of the adjacent resonant modes can be measured at closely spaced frequencies, leading to a wide band of microstrip antenna based on it. The adjacent resonant modes can match well both in terms of impedance by appropriately tuning the slot parameters and the broadband of the antenna is made compact.

3.3.1 Self-inductance Computation Method

The calculation of self-inductance of the proposed antenna has been done by Eq. (2). with and without consideration of ground plane. The ground plane defining coefficient Kg is considered for calculation self-inductance.

The proposed antenna reduces the mutual inductance of geometry using the concept of the negative mutual coupling approach. In this geometry, two directors are used. Self-inductance is analyzed in Tables 1 and 2; the total self-inductance of the top surface is 16.1 mH with a U-Shaped director and

Table 1 — Self-inductance computation of the U-shaped director without consideration of the effect of the ground plane (Kg = 1, height of antenna is 59 mil)

Section of Top Patch	L (mil)	W (mil)	t (mil)	L (mH)
Vertical section 1	20	120	0.08	8.0
Horizontal Section 2	100	20	0.08	1.4
Vertical section 3	120	20	0.08	1.4
Horizontal Section 4	20	100	0.08	6.7
Vertical Section 5	20	100	0.08	6.7
Vertical section 1	20	120	0.08	8.0
Horizontal Section 2	100	20	0.08	1.4
Vertical section 3	120	20	0.08	1.4
Horizontal Section 4	20	100	0.08	6.7
Vertical Section 5	20	100	0.08	6.7
Total Inductance of top surface Patch				48.3
Total Inductance of top surface Patch with U-Slot	100	160	0.08	10.7

Table 2 — Self-inductance computation of the U-Shape Director Consider with Effect of Ground Plane

Section(arms) of U-Shape Director	L (mil)	W (mil)	t (mil)	Kg	L(mH)
Vertical section 1	20	120	0.08	0.3	2.2
Horizontal Section 2	100	20	0.08	0.5	0.8
Vertical section 3	120	20	0.08	0.5	0.8
Horizontal Section 4	20	100	0.08	0.3	2.2
Vertical Section 5	20	100	0.08	0.3	2.2
Vertical section 1	20	120	0.08	0.3	2.2
Horizontal Section 2	100	20	0.08	0.5	0.8
Vertical section 3	120	20	0.08	0.5	0.8
Horizontal Section 4	20	100	0.08	0.3	2.2
Vertical Section 5	20	100	0.08	0.3	2.2
Total Inductance of top surface Patch with U-Slot	100	160	0.08	0.2	1.9

consideration of the effect of the ground plane. Table 1 shows the total self-inductance of the top surface without consideration of the ground plane. Without a U-Shaped director, the total inductance of the geometry is 16.1 mH; the total self-inductance reduces three times when considering the ground plane in an analysis.

Case 1: Computation of mutual between driven element (middle layer) and ground plane (bottom layer)

Case 2: Computation of mutual between director (top layer) and ground plane (bottom layer)

In case 2, the inductance value is optimized much better than the inductance value in case 1 because the interaction between the two coils is negative mutual coupling and the inductance and capacitance of the designed antenna is lower.

3.4 Analytical Modeling of U-Shape Patch(Director)

The U-Shape director is adopted in order to minimize the total mutual induction by enhancing negative mutual induction via the vertical arms of the U-Patch. The arms of currents which run vertically in the same direction produce positive mutual inductance and those which run in opposite direction produce negative mutual inductance. From Fig. 4 (a), l_{e1} is an effective length between the sections 3 & 4, d_{34} are distance between arms 3 & 4. The M_{34} are mutual inductance between arms 3 & 4.

3.4.1 Computation of Negative Mutual Inductance (ΣM_) of U-Shape Patch (Director)

According to greenhouse computation, the positive and negative mutual inductances equations are developed shown from Eqs. (1) - (14) is used to calculate the negative mutual inductance of single U-Shaped patch at the top layer.

$$M_{ab}=\left[2\times10^{-4}l_e\left[\ln\left\{\frac{l_e}{d}+\left(1+\frac{l_e^2}{d^2}\right)^{\frac{1}{2}}\right\}-\left(1+\frac{d^2}{l_e^2}\right)^{\frac{1}{2}}+\frac{d}{l_e}\right]\right]\times K_g \quad \ldots (7)$$

where,

l_e = effective length substitute by the two arms

$$l_e=\frac{l_1+l_3}{2} \quad \ldots (8)$$

For this approximation, l_e considered as an average length between two arms.

d_{13}= Mutual distance between vertical arms 1 and 3.

The developed greenhouse calculation equations for the computation of negative mutual inductance of the proposed antenna are shown from equations 9 to 13 using analysis.

$$M_{15}=\left[2\times10^{-4}l_{e15}\left[\ln\left\{\frac{l_{e15}}{d_{15}}+\left(1+\frac{{l_{e15}}^2}{{d_{15}}^2}\right)^{\frac{1}{2}}\right\}-\left(1+\frac{{d_{15}}^2}{{l_{e15}}^2}\right)^{\frac{1}{2}}+\frac{d_{15}}{l_{e15}}\right]\right]\times K_g \quad \ldots (9)$$

$$M_{13}=\left[2\times10^{-4}l_{e13}\left[\ln\left\{\frac{l_{e13}}{d_{13}}+\left(1+\frac{{l_{e13}}^2}{{d_{13}}^2}\right)^{\frac{1}{2}}\right\}-\left(1+\frac{{d_{13}}^2}{{l_{e13}}^2}\right)^{\frac{1}{2}}+\frac{d_{13}}{l_{e13}}\right]\right]\times K_g \quad \ldots (10)$$

$$M_{24}=\left[2\times10^{-4}l_{e24}\left[\ln\left\{\frac{l_{e24}}{d_{24}}+\left(1+\frac{{l_{e24}}^2}{{d_{24}}^2}\right)^{\frac{1}{2}}\right\}-\left(1+\frac{{d_{24}}^2}{{l_{e24}}^2}\right)^{\frac{1}{2}}+\frac{d_{24}}{l_{e24}}\right]\right]\times K_g \quad \ldots (11)$$

Total Negative Mutual inductance is computed as

$$\Sigma_1^5 M_{\_} = 2M_{\_} \quad \ldots (12)$$

$$M_{\_} = M_{15} + M_{13} + M_{24} \quad \ldots (13)$$

$$\Sigma M_{\_} = 2\Sigma M_{15} + 2\Sigma M_{45} + 2\Sigma M_{24} \quad \ldots (14)$$

The develop computation equation of positive mutual inductance ($\Sigma M_{+)}$ is shown in Eq. 13

$$M_{35} = \left[2\times10^{-4} l_{e35} \left[\ln\left\{ \frac{l_{e35}}{d_{35}} + \left(1 + \frac{{l_{e35}}^2}{{d_{35}}^2} \right)^{\frac{1}{2}} \right\} - \left(1 + \frac{{d_{35}}^2}{{l_{e35}}^2} \right)^{\frac{1}{2}} + \frac{d_{35}}{l_{e35}} \right] \right] \times K_g \quad \ldots (15)$$

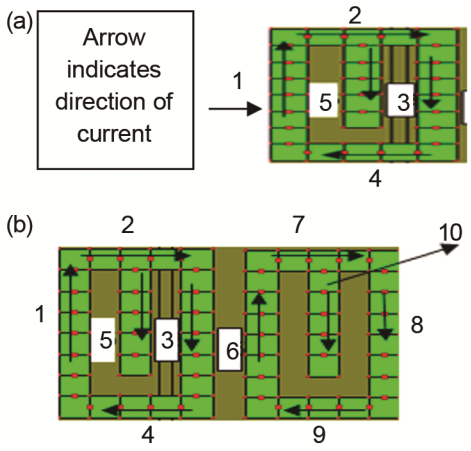

Fig. 4 — (a) Analytical modeling of single U-Shape top Patch (Director); (b) Analytical modeling of two U-Shape Director

3.5 Analytical Modeling of two U-Shaped Patches (Director)

In Fig. 4 (b), the top layer Directors has two U-Shape patches. From Fig. 4, l_{e1} is an effective length of between the sections 3 and 4 and l_{e2} is the effective length of the sections 1 and 6. d_{16} and d_{34} are distance between arms 1 & 6 and arms 3 & 4 respectively. The M_{16} and M_{34} are mutual inductance between arms 1 & 6 and 3 & 4 respectively

3.5.1 Computation of Negative Mutual Inductance

When two U-shaped directors are taken into account, length and average lengths must be computed according to the greenhouse analysis theory for determining mutual inductance.

The Table 3 summarizes the lengths and average lengths of two U-shaped directors. Table 4 shows a summary of the width and average width. Table 5 presents the computation data of negative mutual inductance of the geometry with two U-shaped directors in the radiating patch. The calculation details of the two nearby patches have shown in Tables 3 and 4. Hence for two U=shaped patch negative mutual inductance compute as:

$$M_{\_} = M_{15} + M_{13} + M_{24} + M_{110} + M_{18} + M_{36} + M_{68} + M_{610} + M_{79} + M_{56} \quad \ldots (16)$$

The value of total negative mutual inductance of the designed antenna with the effect of the ground plane is computed to be 2*8.58=17.16mH. The length

Table 3 — Length of Geometry -II

Length of the section	Value (mil)	Length of the section	Value (mil)	Average Length of the section	Value (mil)
L6	20	L10	20	L(6,10)	20
L6	120	L8	120	L(6,8)	120
L9	100	L7	100	L(7,9)	100
L1	20	L5	20	L(1,5)	20
L1	120	L3	120	L(1,3)	120
L2	100	L4	100	L(2,4)	100
L1	20	L10	20	L(1,10)	20
L1	20	L8	20	L(1,8)	20

Table 4 — Width of Geometry –II

Width of the section	Value (mil)	Width of the section	Value (mil)	Average Width of the section	Value (mil)
W6	120	W10	100	W(6,10)	110
W6	120	W8	120	W(6,8)	120
W7	100	W9	100	W(7,9)	100
W1	120	W5	100	W(1,5)	110
W1	120	W3	120	W(1,3)	120
W2	100	W4	100	W(2,4)	100
W1	120	W10	100	W(2,5)	110
W1	120	W8	120	W(1,8)	120

Table 5 — Negative mutual inductance calculation of the geometry-II

Spacing between Elements	Value (mil)	Kg	Mutual Inductance (mH)	Mutual Inductance
d (6,10)	20	0.29	0.56	M(6,10)
d (6,8)	60	0.28	5.45	M(6,8)
d (7,9)	120	0.32	2.57	M(7,9)
d (1,5)	20	0.3	0.56	M(1,5)
d (1,3)	60	0.28	5.45	M(1,3)
d (2,4)	120	0.32	2.57	M(2,4)
d (1,10)	120	0.3	0.099	M(1,10)
d (1,8)	180	0.28	0.061	M(1,8)
Total Negative Mutual inductance				17.32mH

Table 6 — Length calculation of geometry –II

Length of the section	Value (mil)	Length of the section	Value (mil)	Average Length of the section	Value (mil)
L9	100	L10	20	L(9,10)	60
L8	20	L10	20	L(8,10)	20
L4	100	L5	20	L(1,3)	60
L3	20	L5	20	L(3,5)	20
L5	20	L10	20	L(5,10)	20
L3	20	L8	20	L(3,8)	20
L1	20	L6	120	L(1,6)	70
L5	20	L8	20	L(5,8)	20

Table 7 — Width of geometry –II

Width of the section	Value (mil)	Width of the section	Value (mil)	Average Width of the section	Value (mil)
W9	20	W10	100	W(9,10)	60
W8	120	W10	100	W(8,10)	110
W4	20	W5	100	W(4,5)	60
W3	120	W5	100	W(3,5)	110
W10	100	W5	100	W(5,10)	100
W3	120	W8	120	W(3,8)	120
W1	120	W6	120	W(1,6)	120
W5	100	W8	120	W(5,8)	110

and width of the top U-shaped director have been shown in Tables 3 and 4. The distance between the elements and respective calculated negative mutual inductance has shown in Table 5.

3.5.2 Computation of Positive Mutual Inductance

For computation of positive mutual inductance of Geometry –II shown in Fig. 4 (b). The mutual length & width due arms are calculated and shown in Tables 6 and 7

Table 8 provides the calculation summary of the self-inductance, positive mutual inductance, negative mutual inductance, and total inductance of Geometries I and II.

Based on the analysis, it may be noted that the addition of more U-shaped directors has a major influence on the inductive coupling behavior of the antenna. The findings suggest that Geometry V offers the best inductive performance while simultaneously reducing structural complexity; thus, it provides better impedance matching through the proposed antenna system. The improvement in negative mutual inductance enhances the overall impedance bandwidth and radiation characteristics of the antenna. The core aim of this research is to improve the negative mutual coupling. The U-shaped director, which is applied to the top surface, is utilized to add more negative mutual inductance to the antenna structure.

3.6 Inductance Computation in Presence of Ground Plane

The Equations[17] is developed base on the lumped element theory[19] are used to compute the effect of the

Table 8 — Calculation Summary of inductance for geometry I and II

Antenna Geometry	No of U-Shaped Director	Total Self Inductance (mH)	Total Positive Mutual inductance(mH)	Total Negative Mutual inductance(mH)	Total Inductance of the top layer (mH)
I	1	8	12.26	17.16	3
II	2	16.1	14.35	17.32	10.15

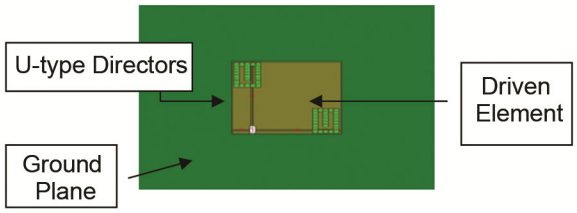

Fig. 5 — Optimization Model for Geometry-I

ground plane on the inductance of the antenna geometry.

The Lmg is the total mutual inductance either computed between driven element and ground plane or between director and ground plane.

where

h= total height of the antenna and as per image theory, the total height of the antenna is taken to be 2h.

L_G = length dimension of the ground plane
C= Dependent correction factor

$$L_{mg} = 2\times10^{-4} L_G \left[\ln\left\{ \frac{L_G}{2h} + \sqrt{1+\left(\frac{L_G}{2h}\right)^2} \right\} + \sqrt{1+\left(\frac{L_G}{2h}\right)^2} + \frac{2h}{L_G} - \sqrt{1+\left(\frac{2h}{L_G}\right)^2} + C \right] \quad \ldots (17)$$

The computation of the correction factor C is based on skin depth δ and width of director or driven element.

$$C = 0.25 \tanh \frac{4\delta}{W} \quad \ldots (18)$$

$$\delta = \frac{1}{\sqrt{\pi\sigma\mu_0}} \quad \ldots (19)$$

This section concluded that most of the impedance matching and radiation characteristics are improved by the U- shaped director of the top layer and ground plane.

3.7 Computation of Probe Inductance

The probe inductance is calculated by the Eq. (20):

$$X_P = \frac{\eta}{\pi} \tan\left(0.5 k_0 h\right) \ln\left(\frac{2.25}{k_0 d}\right) \quad \ldots (20)$$

4 Optimization of Proposed Antenna

The proposed design has been optimized in five sections namely Geometry-I to Geometry-V to enhance the performance of the design in the areas of return loss, impedance bandwidth, and radiation characteristics. The top layer U-type patches have been moved on to five positions to eliminate the mutual coupling in the geometries. Separate detailed discussion is done between Geometry-I and Geometry- V.

i GEOMETRY - I: Two U-type radiating patches will be positioned on the top layer, diagonally left side corner to right side corner

ii GEOMETRY - II: Two U-type radiating patches are placed at the top layer right side corner diagonally to the left side corner of the patch.

iii GEOMETRY: III: A top layer has four symmetrical U-type patches

iv GEOMETRY- IV: There are two radiating patches U-type on the top layer, which are placed near one another

v GEOMETRY - V: Single U-type patch at the left side of the top layer.

4.1. Designing and Analysis of Geometry-I

The Geometry-I involves the use of two U-shaped director patches on the left and on the right sides of the top layer as indicated in Fig. 5. The optimization model of Geometry-I presented in Fig. 5.

4.1.1 Return Losses Vs Frequency (Simulation Results)

The return loss of Geometry I is shown in Fig. 6. It has the -10 dB impedance bandwidth of 5.9 GHz to 16 GHz, 10.1 GHz operating impedance bandwidth, and 17 GHz to 18.5 GHz, the 1.5 GHz operating impedance bandwidth. Highest return losses of up to -20 dB are attained at 12 GHz and 6 GHz.

4.2 Designing and analysis of Geometry –II

The optimized Geometry-II involves the application of two U-shaped Director Patches on the right hand side and the left hand side of the top layer as illustrated in Fig. 7.

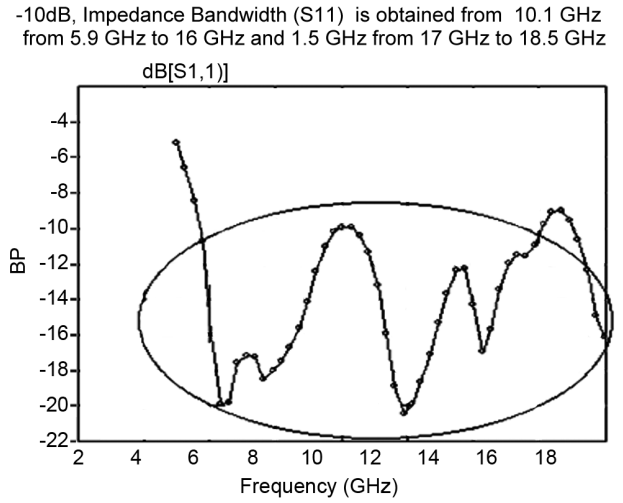

Fig. 6 — Return Losses Vs Frequency

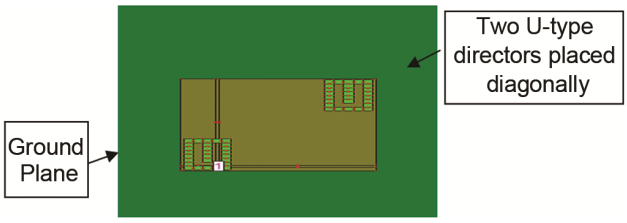

Fig. 7 — Optimization model for geometry-II

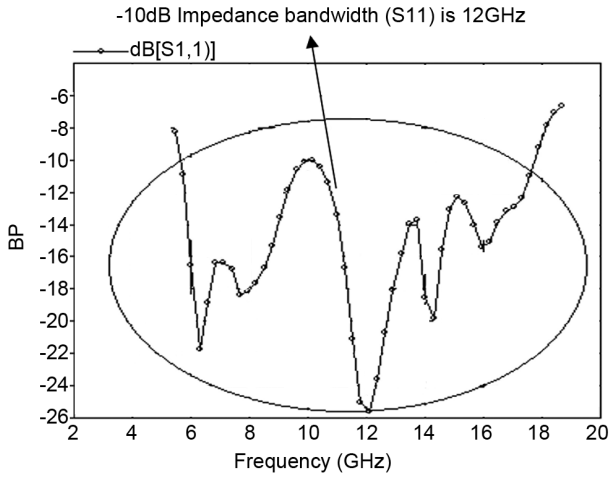

Fig. 8 — Return loss of Geometry -II Vs. Frequency

4.2.1 Return Losses Vs Frequency (Simulation Results)

Figure 8 presents the return loss of Geometry -II. Based on this validation, a -10 dB band of impedance (S11 = -10 dB) of 12GHz was obtained. According to the analysis of the return loss, three notches were realized, the first notch was at 6.2 GHz at -22 dB, the second was at 12 GHz at -26 dB and the third was at 14.2GHz at -20 dB. The negative mutual inductance of the antenna gets enhanced due to the orientation of the U-type radiating patch and results into the overall enhancement of the impedance bandwidth to 15.83 % over the Geometry-I.

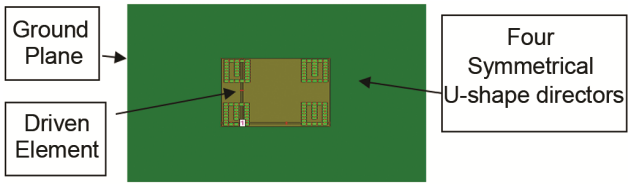

Fig. 9 — Optimization model for geometry –III

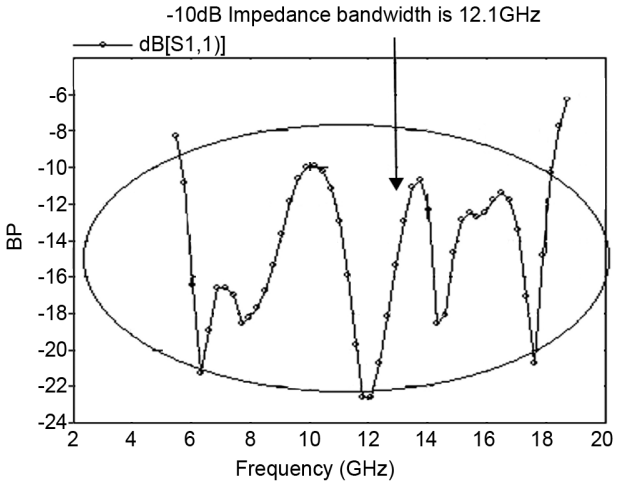

Fig. 10 — Return losses of Geometry-III Vs Frequency

4.3 Designing and Analysis of Geometry –III

Under this optimization sub-section, the four U-Slots are attached on all four corners of the radiating patch as indicated in Fig. 9. The two U-Shaped director patches to the left side and two U-slots to the right side of the top layer have been laid out. Geometry -III Optimization Model is presented in Fig. 9.

4.3.1 Return Losses vs Frequency (Simulation Results)

Figure 10 has indicated the return loss of geometry -III. The highest -10 dB impedance bandwidth has been obtained was 12.1 GHz and the amount of return losses was obtained was also up to -22.2 dB. The orientation of the U-type radiating patch gives enhanced negative mutual inductance of the antenna such that overall bandwidth of the impedance is enhanced to 0.08 % compared with the past geometry yields

4.4 Designing and analysis of Geometry-IV

The Optimization Model of Geometry-IV involves the application of two U- shaped director patches on the left section of the upper layer as illustrated in Fig. 11. The proposed geometry is verified with the help of IE3D simulator.

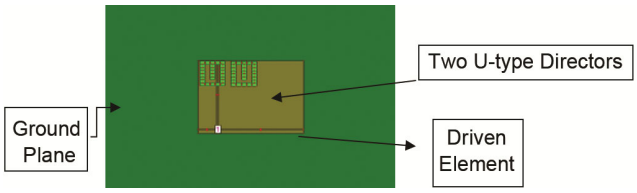

Fig. 11 — Optimization Model for geometry –IV

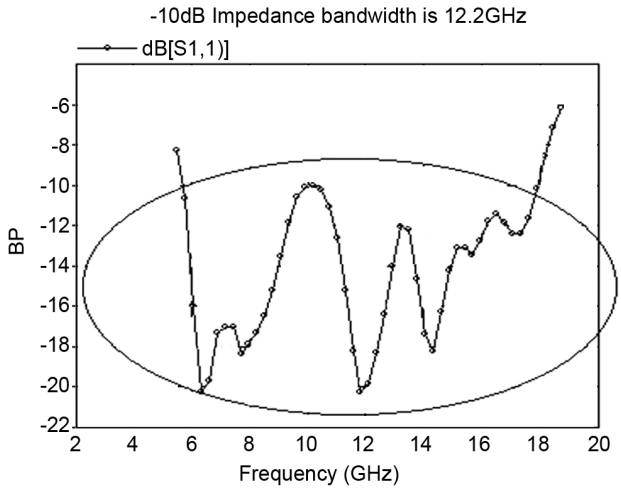

Fig. 12 — Return losses vs. Frequency

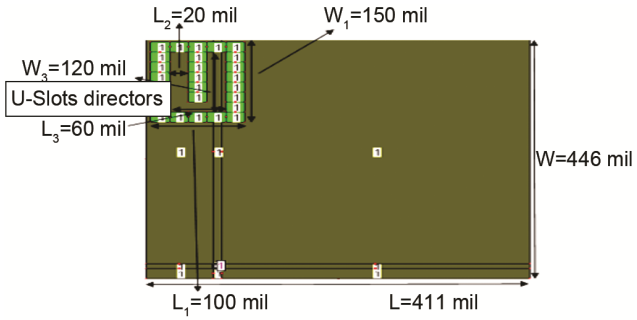

Fig. 13 — Optimization Model of Geometry-V

4.4.1 Return Losses Vs Frequency (Simulation Results)

In Fig. 12, the return loss of Geometry Two is presented. Out of validation, -10 dB of impedance bandwidth has been achieved up to 12.2 GHz. The overall imp of the bandwidth is bettered to 0.08 % than the Geometry-IV.

4.5 Designing and Analysis of Geometry –V

The Geometry-V involves the application of a single U- shaped Director on the left side of the top layer has been presented in Fig. 13. In the comparison of all the five geometries, Geometry -V has a considerable mutual coupling reduction as compared to all the five geometries. Total inductance is optimized up to 10.15mH and with two U-shaped Directors, total inductance is optimized to a value of

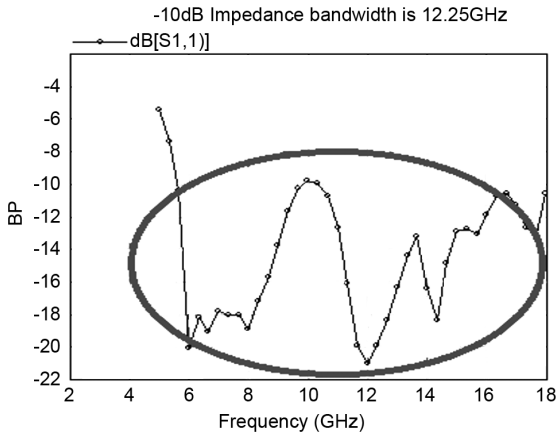

Fig. 14 — Return Loss Vs Frequency

3 mH, thus, the mutual coupling efficiency is three times more optimized with a single U-Shaped Director than with two U-Shaped Directors.

4.5.1 Return Loss Vs Frequency (Simulation Results)

The Geometry –V gives a 12.25 GHz, -10 dBi impedance bandwidth slot that is between 5.8 GHz and 18.17 GHz, as shown in Fig. 14; The return loss at 12 GHz is -21 dBi and at 6 GHz, it is -20 dBi. As the orientation of the U-type radiating patch is changed, the negative mutual inductance of the antenna doubles, and the total impedance bandwidth improves to the 0.04 % relative to the Geometry-IV.

5 Results and Discussion

The Table 9 shows the stepwise increase in the impedance bandwidth achieved as the antenna optimization process continued. The first architecture (Geometry–I) offers -10 dB of impedance bandwidth at 10.1 GHz (5.9 16 GHz) and an added bandwidth at 1.5 GHz (1718.5 GHz). This is the configuration taken as the reference design in further optimization. Geometry-II improves the coupling structure by adding parasitic components and maximizing the bandwidth of the impedance up to 12 GHz, which is a 15.83 percent improvement over Geometry-I. More geometrical improvements, such as manipulation of the U-Shaped Director and parasitic element separation, result in small increments in bandwidth of Geometry-III and Geometry-IV. Lastly, Geometry–V has the highest impedance band width of 12.25 GHz and this shows both the negative mutual coupling and parasitic array techniques have been provided satisfactory outcomes. The Directivity, axial ratio bandwidth, antenna and radiating efficiency have been

Table 9 — Impedance Bandwidth Improvement during Antenna Geometry Optimization

Propose Geometry/Parameters	-10 dB, Impedance Bandwidth	Percentage of Improvement in Impedance Bandwidth after optimization
Geometry-I	10.1GHz (5.9GHz to 16GHz), 1.5GHz (17GHz to 18.5GHz)	In optimization, Geometry–I is considered as the reference design
Geometry-II	12GHz	15.83% better than Geometry–I
Geometry-III	12.1GHz	0.83% better than Geometry–II
Geometry -IV	12.2GHz	0.826% better than Geometry-III
Geometry-V	12.25GHz	0.41%, better than Geometry-IV

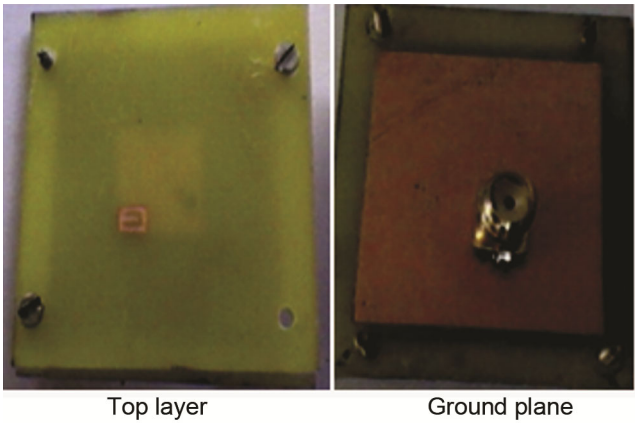

Fig. 15 — Fabricated antenna

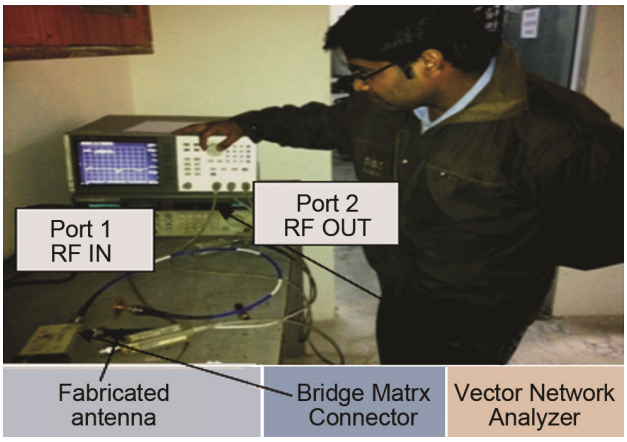

Fig. 16 — Return Loss Measurement setup

analyzed in this section as far as final concluded geometry-v is concerned. The bandwidth and other antenna parameters are being enhanced by the geometries between Antenna- I and Antenna- V. Based on the simulation results of Antenna-I, it can be deduced the negative mutual inductance of antenna is significantly improved overall performance of the antenna.

5.1 Fabrication and Hardware Validation of Proposed Antenna

The proposed Geometry-V has fabricated and demonstrated in Fig. 15. The CAD simulator is used for creating layout of the design antenna. Forthe fabrication, choose two FR-4 glass epoxy substrate and both are inter-connected with air gap of 3 mils. The fabrication process carried out using a standard procedure of photolithography was followed by using a ferric chloride (FeCl 3). All the measurements were performed in controlled laboratory conditions in order to obtain reliable results.

5.2 Return loss and VSWR Measurement

The performance of the proposed ultra-wideband parasitic circularly polarized patch antenna is checked by comparing simulated and acquired results of the reflection coefficient S11. The antenna was first optimized by designing and optimizing a full-wave electromagnetic simulation tool and then optimized geometry was fabricated on the substrate of choice to test the design. To measure the antenna prototype, the antenna prototype was interface with a bridge matrix connector and Vector Network Analyzer (VNA) with 50 Ω SMA connector and coaxial cable as indicated in Fig. 16. These measurements were in controlled laboratory conditions so as to reach out to reliable results. In Fig. 16, the simulated and measured S11 characteristics of the proposed antenna are compared. The findings indicate that the antenna has an ultra-wide impedance bandwidth of 5.8 GHz to 18.15 GHz which covers the C-band, X-band, and Ku-band frequency bands. The return losses were less than -10 dB throughout the operating band, which shows that the impedance matching is good between the antenna and the feeding transmission line. The comparison of geometry I V results has been introduced in all the cases in Fig. 17. All the five geometries have provided successful Ultra-wide bandwidth. Geometry II was found to have low impedance bandwidth as compared to Geometries I, III, and IV (over 12 GHz). Simulated and measured are close to each other. The conclusions are drawn and it has been established that the proposed antenna design is valid methodology. There are small differences in the curves which are

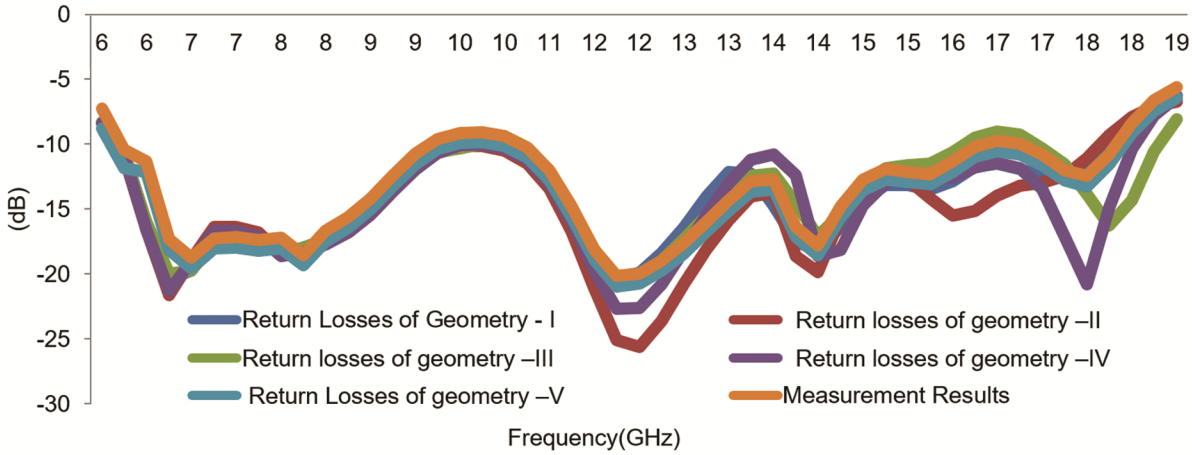

Fig. 17 — Return Loss of the Fabricated Antenna

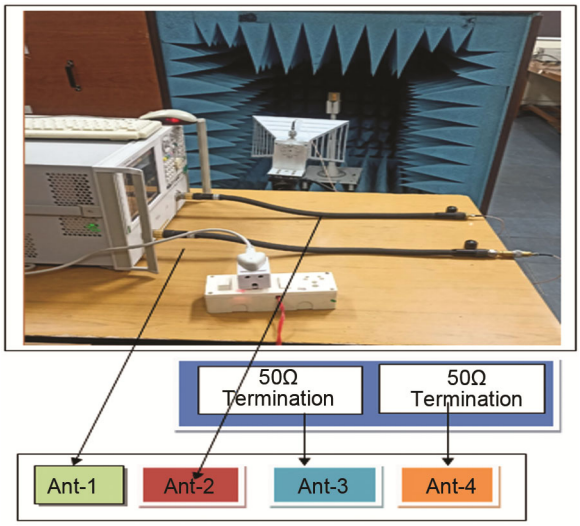

Fig. 18 — Measurement setup of the Radiation Pattern

attributed to tolerances in fabrication, variations of dielectric constant of substrate. Findings on Geometry I to Geometry V have been presented in Fig. 17. All five Geometries have resulted in effective ultra-wide bandwidth. The results were discussed according to returned losses (S11≤-10 dB) and percent impedance bandwidth. All geometries had reported an impedance bandwidth exceeding 12 GHz, except geometry II.

5.3 Measurement Setup for Testing of the Radiation Pattern

The radiation pattern of the design antenna is measured with the help of the microwave anechoic chamber shown in Fig. 18. Experiment was carried out in real conditions of electromagnetic measurements. Pyramidal RF absorbing materials coded on the chamber walls and suppress the electromagnetic reflections and cause outside interference. The return losses, VSWR coefficient and radiation pattern of the fabricated antenna is measure using a Vector Network Analyzer (VNA). A coaxial RF cable with 50Ω termination is used to interface antenna and Vector Network Analyzer. The VNA is then calibrated to a standard Open-Short-Load (OSL) method before measurements are taken to remove systematic errors in measurements caused by cables and connectors. The AUT lies within the anechoic chamber of the center of the chamber on non-conductive support platform. There is a standard horn antenna in front of the AUT and which is used as transmitting/receiving reference antenna in the determination of radiations. Measurement of radiation pattern of the antenna measure under far field zone conditions

5.4 Directivity Vs Frequency Analysis for Geometry -I to Geometry –V

The Directivity of Antenna varies from 5 dBi to 11.5 dBi for Geometry-I to Geometry-V. The Directivity show in Fig. 19 varies from 5 dBi to 11.5 dBi. All Geometry has been reported maximum directivity up to 11.5 dBi at 16 GHz.

5.5 Axial Ratio Vs Frequency for Geometry -I to Geometry-V

The geometry optimization of the proposed antenna was analyzed by the axial ratio (AR) properties of the antenna to determine the circular polarization behavior of this antenna. The axial ratio shows the purity of the circular polarization of the antenna in which AR values below 3 dB indicate good circular polarization. Figure 20 shows axial ratio analysis from Geometry I to Geometry V. With a Geometry-I configuration, the values of the axial ratios vary and they are relatively higher in the introduction of

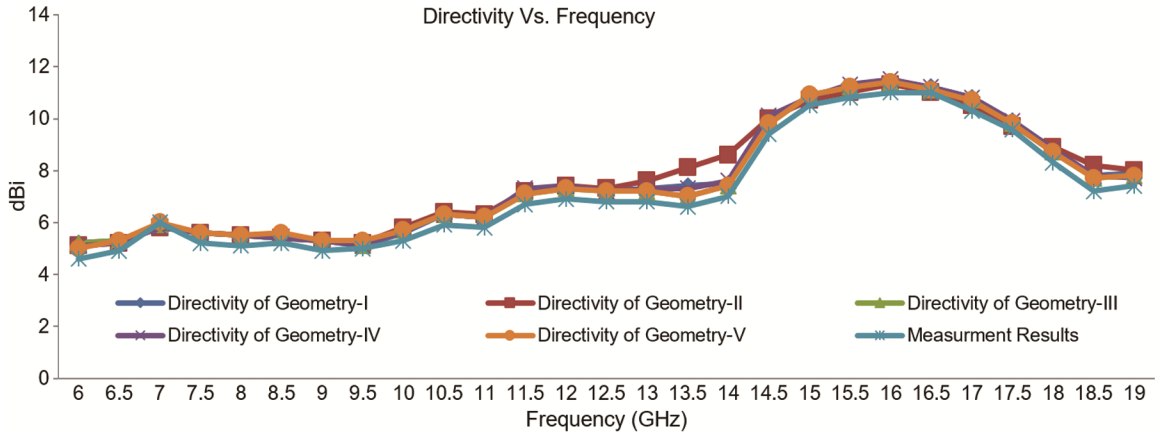

Fig. 19 — Directivity Vs Frequency analysis

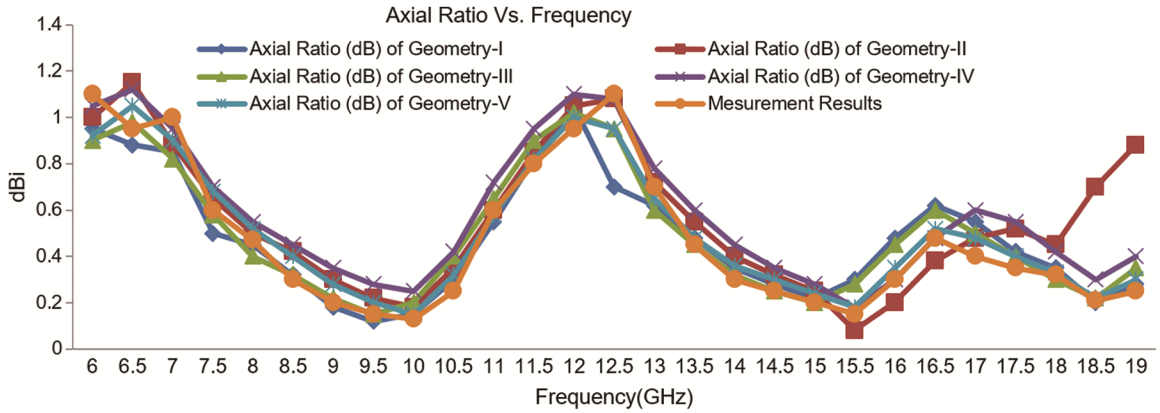

Fig. 20 — Axial Ratio Vs Frequency analysis

Geometry II and the parasitic element, there is enhanced performance of the axial ratio as the Geometry II has added features in terms of gap coupling, and the electromagnetic coupling between the driven element and the directors, is enhanced by the presence of the parasitic element. The U-Shaped Director geometry and the distance between parasitic elements in Geometry III and Geometry IV are further optimized to produce the improved orthogonal current components which are necessary in the generation of the circular polarization. Lastly, the Geometry-V optimized antenna design has the smallest and stable values of axial ratios over the operating band, and it has shown a good performance of circular polarization.

In order to check the results represented by the simulation, the optimized antenna prototype (Geometry V) was built and tested experimentally. Measurement of axial ratios was done in anechoic chamber arrangement with a standard horn antenna as a reference antenna. The measured values of the axial ratio are in good faith with the simulated value, with just small deviations being noticed owing to fabrication tolerances, connector losses as well as measurement uncertainties. The fact that simulated and measured axial ratio values are closely correlated proves that the negative mutual coupling process and the new U-shaped parasitic directors are efficient to increase the performance of circular polarization of the proposed antenna. Thus, the antenna will be applicable in the wireless communication of C-band, X-band and Ku-band. The 1 to 5 ratio axial of the geometry has been demonstrated in Fig. 19, the 3dB, axial ratio bandwidth of all geometry and provides the circular polarization. Geometry-I to Geometry-V: Circular polarization bandwidth (axial ration< 3dB) 2 12GHz and the axial ratio of all geometries is less than 1. 2 dB, and the axial ration 2 3 dB. Geometries I to V have been reported to have > 12 GHz and Geometry IV is highly circularly polarized more than any geometry. Geometry I also has highly circularly polarized at 15. 7 GHz with value of axial ratio is 0. 001 dB and Geometry is most circularly polarized at 17. 6 GHz with axial ratio of value 0. 001 dB.

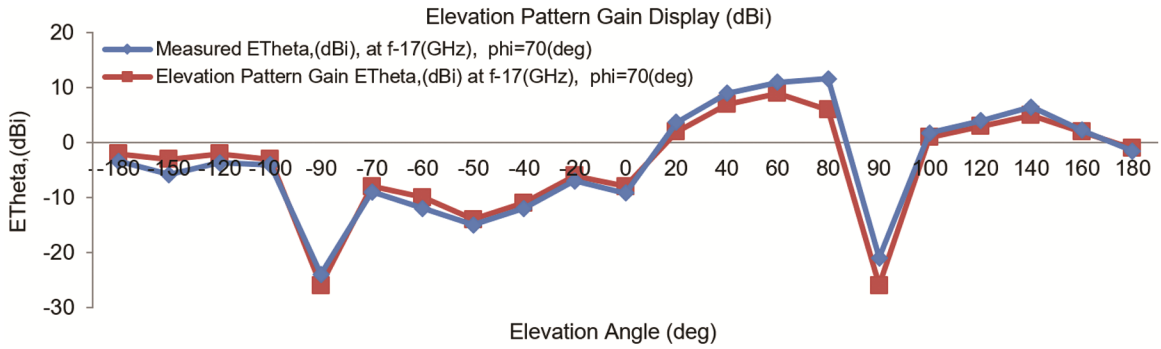

Fig. 21 — Azimuth radiation pattern of the proposed antenna at 6 GHz for θ = 120°

5.6 Radiation Pattern (E–Plane and H–Plane)

Simulation and experimental data were both achieved in the determination of the radiation characteristics of the proposed ultra-wideband parasitic circularly polarized patch antenna. The knowledge of the radiation patterns was obtained in the microwave anechoic chamber with the help of standard horn antenna as a reference antenna. The antenna under test (AUT) was placed on non-conductive rotating platform and transmitting horn antenna was placed in sufficient distance of the far-field of the AUT during the measurement process. The antenna was rotated by a full 360-degree and the radiated power was read at the different angular positions to find the radiation patterns at the E plane and the H plane. The output demonstrates the simulated and experimental radiation distributions of the optimized antenna within some of the characteristic operating frequencies in C-band, X-band and Ku-band. According to the radiation patterns, the antenna has constant directional radiations, which are highly symmetrical both in E- plane and in H- plane. E-plan E-plane pattern demonstrates a large major lobe and low side-lobe values whilst H-plane pattern indicates near Omnidirectional behavior as exhibited by patch antenna systems. Overall, the results confirm that the antenna developed has fixed radiation patterns and gain within the frequency band of operation of 5.8 GHz to 18.15 GHz and hence is applicable in the C-band, X-band and Ku-band wireless communications usage.

5.6.1 Elevation Pattern Gain ETheta, (dBi) at f-17(GHz), phi=70(deg)

The radiation pattern of E -theta polarization (70^0) at 17 GHz also exhibits a clearly directional behavior with a maximum gain of about 9.28 dBi shown in Fig. 21. An elevation angle of 50° to 60 ° forms the center of the main lobe which shows the direction of the maximum radiation. The pattern shows clear nulls at about 90° where the gain is sharply decreased to about -25 to 27 dBi, which implies a small amount of radiations in the directions. Besides the main lobe, some side lobes are seen to occur especially around the angle 120-150 deg with gains of between 3 and 5 dBi and are indicators of the secondary radiation content. The above properties imply that the antenna is very directional in nature with a good amount of radiations blocked in some direction. The simulation and hardware validation results are almost match to each other.

5.6.2 Azimuth Radiation Pattern at 12 GHz (E-phi , θ = 60°)

The azimuth radiation pattern at 12 GHz (E-phi polarization, θ = 60°) shown in Fig. 22, exhibits a directional and asymmetric behavior with a peak gain of approximately 6.7–7 dBi. the maximum fields distribution occurs across the angle 120° to 140° The radiation pattern exhibits notable nulls near −150° and approximately 60°–70°, where the gain diminishes to roughly −12 dBi, signifying minimal radiation in these specific directions. Secondary lobes are present, notably around −130° and 20°–30°, with moderate gain levels of about 2–3 dBi. The gain varies over a wide range from approximately −12 dBi to +7 dBi, and moderate back radiation is observed near ±180°, with gain values close to 0 to −3 dBi. Overall, the pattern indicates a non-uniform and directional radiation characteristic, with energy concentrated in a preferred direction and reduced radiation in other. The simulation and hardware validation results are almost match to each other.

5.6.3 Azimuth Radiation Pattern at 12 GHz (E-phi polarization, θ = 50

The azimuth radiation pattern at 12 GHz (E-phi polarization, θ = 50°) shows in Fig. 23,

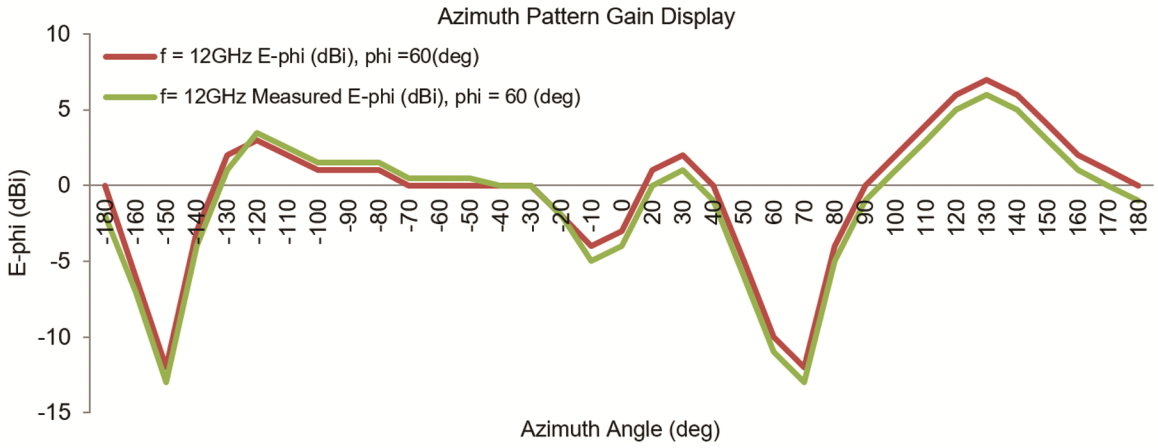

Fig. 22 — Azimuth radiation pattern at 12 GHz (E-phi, θ = 60°)

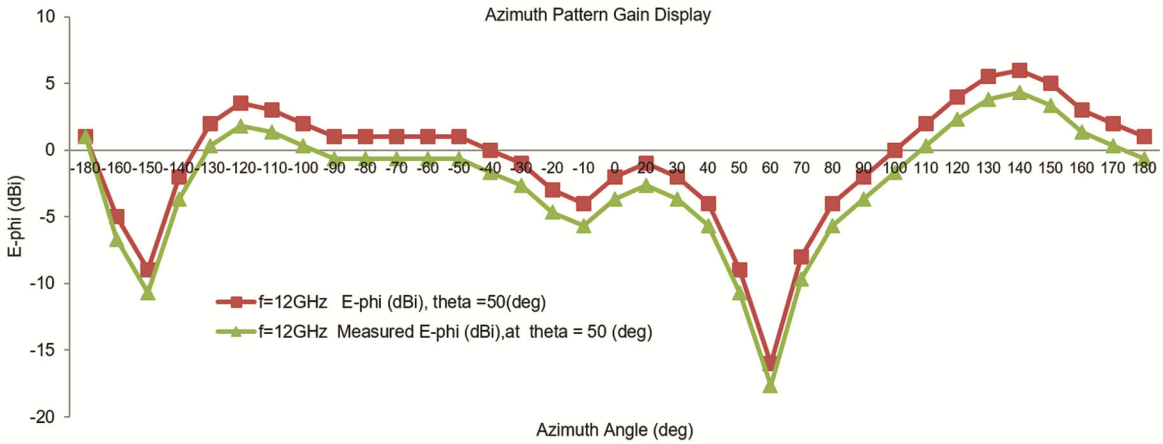

Fig. 23 — Azimuth radiation pattern at 12 GHz (E-phi polarization, θ = 50

exhibits a directional and asymmetric behavior with a peak gain of approximately 5.75–6 dBi. The principal lobe's orientation spans from 130° to 140°, thereby denoting the direction of peak radiation. A pronounced null is apparent around 60°, where the gain undergoes a rapid decrease, reaching approximately −16 dBi, which suggests significant radiation attenuation in that particular direction. Furthermore, a noticeable reduction is detected near −150°, with gain values nearing −9 dBi. Throughout the negative azimuth angles, the gain remains comparatively low and exhibits moderate fluctuations; conversely, a gradual increase is noted as one approaches positive angles, Overall, the pattern demonstrates a directional radiation characteristic, with strong radiation concentrated in a preferred angular region and reduced radiation in other directions due to the presence of deep nulls and side lobes. The simulation and hardware validation results are almost match to each other.

5.6.4 Elevation Radiation Patterns at 6 GHz (E-theta polarization) for φ = 50°

Figure 24 which illustrate the radiation patterns of 6 GHz (E-theta polarization) with 50 and 70 degrees have indicated that the radiation pattern is directional with significant differences in the distribution of gain. The highest peak gain of the antenna is higher with φ = 50^0 at around 2.53 dBi, implying that the higher phi the lower is the efficiency of the radiation. The dominant radiation field. Sharp nulls are found at about 90, and the 70^0 case (compared to 50^0) shows deeper nulls (approximately -26 dBi and -18 to -20 dBi respectively) showing more suppression of the radiation in these directions. The gain then rebounds above 90, especially at 50^0 of the front that a comparatively constant level of radiations (approximately 2-3 dBi) is noticed. In general, the angle 500 pattern has been shown to exhibit improved and smoother radiation performance, except that 700 has less gain and deeper nulls, indicating a more

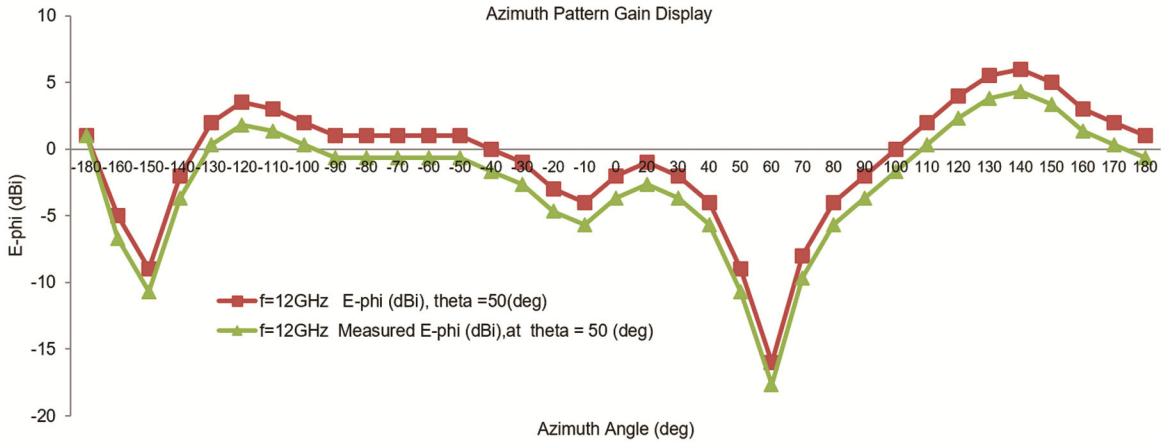

Fig. 24 — Elevation radiation patterns at 6 GHz (E-theta polarization) for φ = 50°

dampened and nonuniform radiation behavior. Validation of a simulation and hardware is almost identical.

5.7 Comparative Analysis

The performance comparison of the proposed antenna and the literature of recently reported antenna designs is discussed. Based on the comparison, it is possible to observe that most of the available antennas are limited in terms of frequency range or offer moderate bandwidth and gain performance. For example, the Metasurface High-Gain Antenna[2], over the frequency range of 6 GHz to 15 GHz, provided an 85 % bandwidth with a gain of 10.1 dBi and linear polarization. The Parasitic Patch with DGS[4], over the frequency range of 5 GHz to 12 GHz, provided an 80 % bandwidth and a gain of 8. 6 dBi with linear polarization. The Hybrid Slot Antenna[5], over the frequency range of 3 GHz to 14 GHz, provided a 95 % bandwidth and a gain of 8 dBi with linear polarization. The Dual-Patch Slot Loaded Antenna[6], over the frequency range of 3 GHz to 14 GHz, increased the impedance bandwidth to 65 % by loading slots, with a gain of 7.1 dBi and linear polarization. The Dielectric Superstrate Microstrip Antenna[7] used a dielectric layer for gain improvement in the frequency range of 5 GHz to 10 GHz and generated a 50 % impedance bandwidth with a gain of 9. 3 dBi. The Compact Wideband Antenna Design[8] was developed to provide a 55 % impedance bandwidth over the frequency range of 4 GHz to 8 GHz with a gain of 6. 8 dBi. The Broadband U-Shaped Director Microstrip Antenna[9] provided a 70 % impedance bandwidth over the 4 GHz to 12 GHz frequency range with a gain of 9 dBi. Nevertheless, most of these designs continue to be limited in terms of bandwidth, linear polarization, or fairly large antenna sizes. Similarly, the antenna suggested by[14] has dual-band operation that matches that of 5G, and the antenna gain and bandwidth have been enhanced by [15] with the help of metasurface. In contrast, the proposed antenna has a much broader impedance bandwidth of 5.8 GHz to 18.15 GHz, implying applications in C-band, X-band, and Ku-band wireless communication. It offers a 102 % impedance bandwidth with a gain of 11.5 dBi and circular polarization. Negative mutual coupling and parasitic array techniques are used to enhance the antenna gain and radiation performance. Additionally, U-shaped directors have been introduced, which increase the radiation properties and facilitate circular polarization, Thus, the proposed antenna demonstrates better performance regarding ultra- wideband, high gain, and circular polarization compared to other reported designs. Both the simulated and experimental outcomes have been found to be quite similar.

6 Conclusion

This paper has presented the mutual coupling reduction technique using greenhouse analysis. The method of calculating self-inductance, Positive, and Negative mutual inductance has been discussed. The appropriate design of the top layer director is generating appropriate negative mutual inductance and optimizes the total inductance of the proposed antenna. The optimization of the proposed antenna has been done in five sections with consideration of the effect of the ground plane. With reference to validation of work, concluded that Single U-Shaped Director significantly producing the negative mutual

inductance and positive mutual inductance to reduce total inductance and mutual coupling inside the antenna geometry. All the five geometry have reported impedance bandwidth up to 12.2 GHz. S11 ≤ -10 dB response between 5.8 GHz to 18.17 GHz has been achieved 102 % BW, and utilized 38 % BW for X-Band, 19 % BW for C – Band, and 45 % BW for Ku –Band. The propose geometry is provided directivity 5d Bi to 11.3 dBi over 12.2GHz impedance bandwidth slot, achieved, 60 % to 100 % radiating efficiency, 50 % to 95 % antenna efficiency and 3dB. Axial bandwidth up to 12.2 GHz. The Proposed antennas are highly circular polarized antennas and the circular polarization bandwidth (axial ratio ≤ 3 dB), is ≤ 12 GHz, this proposed antenna can be used for X-Band, Ku Band, and C-Band applications. The Hardware results are validated and found similar.

References

1 Lou S, Qian S, Lian S, Wang W, Bao H & Leng G, *IEEE Trans Antennas Propag*, 73 (6) (2025) 3628.
2 Hassan M & Abbas K, *IET Microwaves, Antennas Propag*, 19 (2) (2025) 221.
3 Balamurugan B C, *et al.*, *Scientific Rep*, 15 (2025) 3423.
4 Gupta P & Sharma V, *IEEE Access*, 13 (2025) 45231.
5 Chen Y & Zhao L, *IEEE Trans Antennas Propag*, 73 (1) (2025) 312.
6 Park S & Kim J, *IEEE Access*, 12 (2024) 14652.
7 Rahman M & Islam A, *Optic Quant Electron*, 56 (5) (2024) 1.
8 Verma K & Kumar P, *IEEE Access*, 12 (2024) 78901.
9 Liu Y, Wang Y & Zhao J, *IET Microwaves, Antennas Propag*, 18 (2) (2024)134.
10 Laller R, Abegaonkar M P & Basu A, *Proc IEEE MAPCON*, 2024 pp. 3–7.
11 Diaha K C F, Karami F & Boutayeb H, in *Proc ICCIMS*, 2024 p. 6–9.
12 Adriansyah M A, Wahdiyat A I & Apriono C, in *Proc FORTEI-ICEE*, 2024 pp. 130–135.
13 Odabasi H, Salimitorkamani M & Turan G, *IEEE Antennas Wireless Propag Lett*, 22 (11) (2023) 2899.
14 Alwan, Sali A, Abdullah J & Ali A, *IEEE Access*, 11 (2023) 72521.
15 Zhou X, Deng L & Zhang Y, *IEEE Trans Antennas Propag*, 71 (3) (2023) 2267.
16 Nguyen T & Lee K, *IET Microwaves, Antennas Propag*, 17 (4) (2023) 512.
17 Nema R, *Int J Antennas Propag*, 2014 (2014) 1.
18 Nema R, *Int J Microwave Wireless Technol*, 5 (S1) (2013) 77.
19 Bahl I, Lumped Elements for RF and Microwave Circuits, Boston, MA, USA, 2003 pp. 55–60.
20 Greenhouse H M, *IEEE Trans Parts, Hybrids Packag*, 10 (2) (1974) 101.
21 Suman P N & Mishra G K, *AEU - Int J Electron Commun*, 184 (2024) 1.
22 Suman P N, *et al*., *IETE J Res*, (2024) 1–10.